Conceptual Design of a Gulled-Wing Commercial Transport

Robert B. Taylor [1]
NASA Langley Research Center, Hampton, VA, 23681

Open rotor powerplants have long been discussed as a potential solution to reduce aircraft fuel burn by increasing effective bypass ratio. However, this promising technology presents unique integration challenges. A gulled-wing approach for commercial transports is proposed to accommodate large-diameter powerplants. Integration effects of open rotor powerplants are modeled, analyzed, and discussed. Aerodynamic analysis and refined structural weight estimates are used to inform a preliminary conceptual design. Mission analysis of this model is performed, and the results are compared against NASA's 154-passenger N+3 Conventional Configuration advanced technology baseline. Results indicate that gulled wings are a viable solution for integrating large powerplants. Application of an open rotor engine model resulted in a fuel burn benefit on the order of 15% compared to the conventional turbofan configuration.

I. Nomenclature

$C_{D_{interference}}$	=	interference drag coefficient
C_{D_f}	=	friction drag coefficient
$C_{D_{f/power\ off}}$	=	power-off friction drag coefficient
$C_{D_{f/power\ on}}$	=	power-on friction drag coefficient
$C_{fuselage}$	=	fuselage circumference
c_{f_c}	=	component flat-plate friction coefficient
c_{wash}	=	chord of wing at engine centerline
$D_{fuselage}$	=	fuselage maximum diameter
D_{rotor}	=	rotor diameter
dz_{pylon}	=	vertical distance from wing chord to top of nacelle
E_A	=	minimum shielding absorption energy
FF_c	=	component form factor
k	=	friction drag correction factor for compressibility
L	=	presented blade perimeter at impact
L_z	=	vertical component of lift vector
$l_{main\ gear}$	=	length of main landing gear
M_{DD}	=	Mach drag divergence number
r_{debris}	=	distance between engine centerline and fuselage skin
$r_{nacelle}$	=	nacelle maximum radius
r_{rotor}	=	rotor radius
$S_{inboard}$	=	wing planform area inboard of engine centerline
$S_{outboard}$	=	wing planform area outboard of engine centerline
S_{ref}	=	aircraft reference area
S_{wet_c}	=	component wetted area
$S_{wet_{nacelle}}$	=	nacelle wetted area
$S_{wet_{wing/Total}}$	=	total wing wetted area
$S_{wet_{wing/clean}}$	=	wing wetted area experiencing freestream conditions
$S_{wet_{wing/wash}}$	=	wing wetted area experiencing flow from the rotor wash

[1] Aerospace Engineer, Aeronautics Systems Analysis Branch

S_{wing}	=	wing planform area
T	=	fuselage shielding dynamic shear modulus
$t_{shielding}$	=	fuselage shielding thickness
v_{impact}	=	rotor blade impact velocity
w_{blade}	=	rotor blade weight
$w_{shielding}$	=	fuselage shielding weight
y_{engine}	=	engine y location
$y_{MAC/inboard}$	=	inboard wing section mean aerodynamic chord y location
$y_{MAC/outboard}$	=	outboard wing section mean aerodynamic chord y location
$y_{wing/root}$	=	wing root y location
z_{engine}	=	engine z location
$z_{wing/root}$	=	wing root z location
$\Delta C_{D_{interference/power\ on}}$	=	change in interference drag due to rotor power-on effects
δ	=	wing dihedral
$\delta_{avg/Target}$	=	target area-weighted average dihedral
$\delta_{inboard}$	=	wing dihedral inboard of engine centerline
$\delta_{outboard}$	=	wing dihedral outboard of engine centerline
θ_{debris}	=	rotor blade debris spread angle
θ_{impact}	=	angle between rotor blade body axis and point of impact
$\rho_{shielding}$	=	fuselage shielding material density

II. Introduction

A. Motivation

Commercial aviation accounts for 2.4% of global CO_2 emissions [1]. More than sixty percent of daily commercial flights are flown on narrowbody-class transports that carry between 120 and 200 passengers. The International Council for Clean Transportation estimated that aircraft of this category alone are responsible for more than half of aviation emissions [2]. Recent years have witnessed a growing interest in developing and applying advanced engine, aerodynamic, structural, and operational technologies to reduce global emissions. A reduction of even a few percent in mission fuel burn for aircraft of this category would have substantial benefits, with the potential to reduce airline operating costs, passenger ticket prices, and above all, aviation emissions.

B. Background

High bypass ratios (BPRs) are known to improve propulsive efficiency for turbofan engines. Generally, as a fan's BPR increases so must its diameter. As BPR increases, the weight of and drag produced by necessarily larger nacelles start to negatively impact system-level efficiency [3]. Open rotors (ORs) circumvent this roadblock entirely by removing the fan duct. ORs, also known as unducted fans, propfans, and open fan engines, enable far greater propulsor diameters by reducing nacelle installation effects [3].

ORs are not without their own set of integration challenges. With far larger diameters than conventional turbofans and exposed rotor blades, they cannot simply be swapped with the engines of today's low-wing, narrowbody aircraft. Although high-wing and rear-mounted configurations may alleviate some of these integration challenges, both have their own drawbacks and tradeoffs. Longer landing gear may provide the necessary ground clearance with a low-wing configuration but incur a weight penalty, require reconfiguration of the fuselage to meet volume requirements, and are louder when deployed. The B737-10 MAX illustrates the difficulties of integrating longer landing gear, where a significant engineering effort was undertaken to increasing landing gear length by 10 inches without fuselage modifications [4]. There are also several other constraints on OR engine location. Section IV.B highlights that the cross-engine debris, rather than ground clearance, may be the dominant constraint on the engine's vertical location. Additionally, the introduction of accelerated flow over the wing at transonic speeds will incur a significant aerodynamic penalty if not properly considered. As the wing must already be modified for this reason, raising the engine with a slight "gull angle" in the process has the potential to resolve many of these constraints. With the increased inboard dihedral illustrated in Fig. 1, the 154 passenger Gull Wing (GW154) concept provides greater ground clearance for the same length landing gear, reduces the risks of exposed rotor blades, and requires minimal fuselage reconfiguration as compared to its high-wing and rear-mounted counterparts.

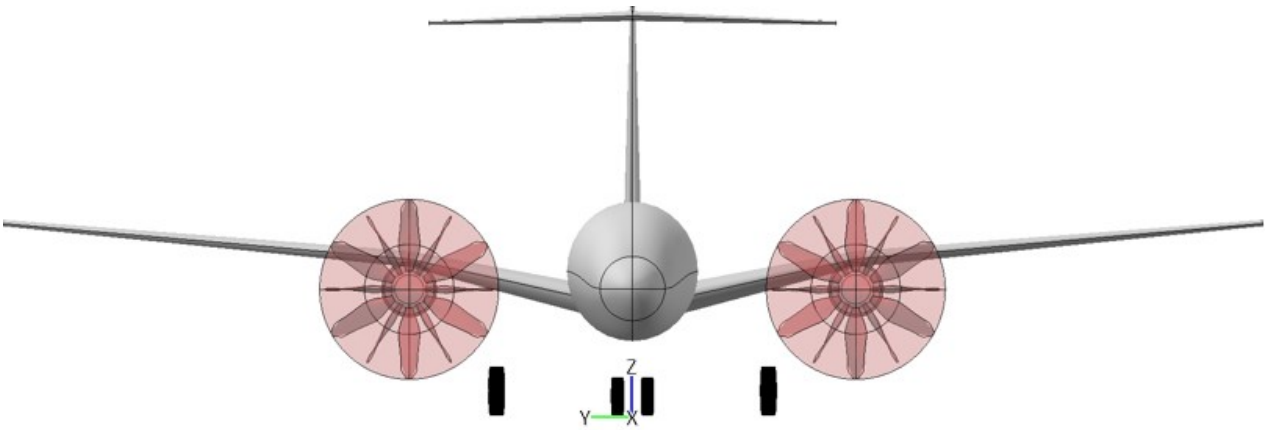

Fig. 1 Front view of GW154 concept with reference coordinates.

C. Scope

This paper focuses on evaluating a gulled-wing configuration with an OR powerplant. It uses the GW154 to highlight the integration challenges associated with an OR and quantify the aircraft-level efficiency gains relative to a conventional, turbofan-powered technological peer. NASA's 154-passenger N+3 Conventional Configuration (N3CC) aircraft concept serves as the advanced technology baseline [5]. Further discussion of this concept can be found in Section III. High-wing and rear-mounted concepts were not considered, though these configurations may be examined in future work.

The modeling effort and design constraints are consistent with those of the N3CC. Technology assumptions are based on a 2035 entry into service (EIS). In the interest of speed and consistency, low fidelity design and analysis tools are used wherever possible. Mid-fidelity analyses are employed where lower-order methods do not fully capture the unique characteristics of this concept. OpenVSP [6] is used to model the GW154 geometry. NASA's Flight OPtimization System (FLOPS) [7] is used to perform aircraft sizing and mission analysis. Trade studies and concept optimization are conducted using a framework developed from OpenMDAO, an open-source high-performance computing platform for systems analysis and multidisciplinary optimization [8].

The GW154 is designed to minimize fuel burn. Though real-world objective functions are significantly more complex, fuel burn is used as a rough proxy for both operating cost and block emissions. Takeoff gross weight (TOGW) is used to approximately capture acquisition cost when evaluating tradeoffs. Block fuel consumption is the primary metric for evaluation against the baseline, but the discussion of results is more nuanced. Structural weight, performance relative to other potential integration solutions, and intangibles such as maintainability, reliability, and consumer acceptance are used to contextualize this concept.

Section III discusses the baseline aircraft and mission requirements. The conceptual design approach is described in Section IV. This includes explanations of the modeling efforts, assumptions, and rationale, along with the trade studies and reasoning behind major design decisions. Section V describes the sizing and analysis methodology. Section VI presents the sizing and mission analysis results and compares them to those of the baseline. Section VII contains the concluding remarks.

III. Baseline Aircraft and Mission Requirements

The GW154 is designed to replace narrowbody subsonic transports currently in service, such as the B737-8 MAX or A320neo. NASA's N3CC was developed to be representative of a conventional narrowbody aircraft with an EIS date of 2035. The model incorporates "N+3" technologies and is periodically updated to reflect recent advancements. It serves as a baseline against which the performance of advanced transport concepts can be evaluated. It is powered by an "Advanced Turbofan" (AT) propulsion model, developed under a separate effort to represent the expected state-of-the-art (SOA) of turbofan engine technology with a 2035 EIS. To ensure a fair comparison, the same set of design requirements and performance constraints imposed on the N3CC, found in Table 1, are applied to the GW154. The values selected are based on those typical of current aircraft of this class.

With the same requirements and constraints as the N3CC, it follows that the GW154 would best be sized using the N3CC as a starting point. Other than the engine, wing, and landing gear, the configuration and technology assumptions remain unchanged. Initial geometries and weights are taken directly from the N3CC models in OpenVSP and FLOPS.

Table 1 Design Requirements

Requirements	Value	Units
Design Mach	0.8	-
Min. Altitude at Top of Climb	36,000	ft
Min. Climb rate at Top of Climb	300	ft/min
Design Range	3,500	nmi
Passenger Capacity	154	seats
Design Payload	33,880	lb
Max. Wingspan	118.1	ft

IV. Concept Design

A. Propulsion Model

The engine model was developed as part of NASA's Hybrid Thermally Efficient Core (HyTEC) project [9]. Through HyTEC, NASA is coordinating with industry partners to develop and assess next-generation aircraft propulsion technologies. The Vision Open Rotor (VOR) model used in this study was created to enable an independent assessment of OR concepts based on technology projections for an EIS of 2035. This engine is intended to power the next generation of narrowbody transports. Its thrust characteristics closely match those of CFM's LEAP-1B28 engine, which serves as the baseline engine for the VOR [9].

The VOR has a single rotor followed by a set of swirl recovery vanes (SRVs) to straighten the rotor wash and recover some of the kinetic energy lost to circulatory motion. The pitch of both sets of blades can be varied depending on flight conditions and throttle setting. Past OR engine concepts have incorporated two sets of rotors per engine rotating in opposite directions to reduce swirl-induced losses, but the costs of increased noise, mechanical complexity, and weight were deemed too great [10]. Figure 2 shows a side view of the VOR with the assumed thrust and drag domains. The aerodynamic characteristics of the VOR are discussed in greater detail in Section III.C.

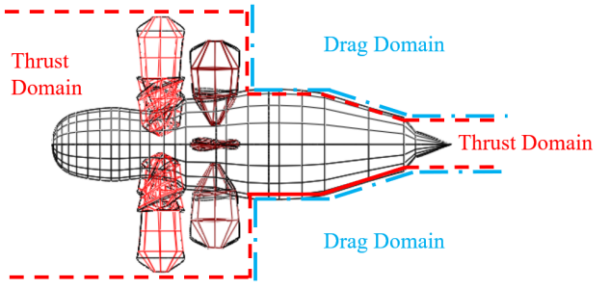

Fig. 2 Diagram of thrust and drag domains assumed for HyTEC Vision Open Rotor (VOR).

Several studies on propeller-driven aircraft indicate that an "inboard-up" rotation is aerodynamically optimal as it minimizes the rotor's effect on the wing lift distribution and the associated increase in induced drag [11,12]. The port and starboard engines rotating in opposite directions results in additional gearbox weight and operational challenges. Despite this additional mechanical and operational complexity, the potential aerodynamic gains are assumed to outweigh these penalties.

Cycle modeling was performed using the Numerical Propulsion System Simulation (NPSS) software [13]. Weight estimates were provided using the Weight Analysis for Turbine Engines (WATE++) code [14]. Table 2 presents a comparison parameters for three propulsion systems: the 2019 state-of-the-art (LEAP-1B28), the N3CC Baseline (AT), and the VOR engine. The VOR is heavier and larger than its AT counterpart.

The AT was modeled internally at NASA and has been updated with improved assumptions since the work detailed in Ref. [5]. Although the AT and VOR models both target an EIS of 2035, they were developed under separate efforts. Differences in the underlying assumptions used to construct these models are a source of uncertainty in this study.

Table 2 Comparison of Engine Parameters [9]

Parameter		LEAP-1B28	AT	VOR	Units
Sea Level Static	Net Thrust	29,000	23,281	29,100	lbf
M=0, 0 ft	TSFC	0.31	0.27	0.13	lbm/(hr*lbf)
Cruise	Net Thrust	5,400	3,430	5,400	lbf
M=0.8, 35000 ft	TSFC	0.56	0.53	0.46	lbm/(hr*lbf)
Nacelle Diameter		7.4	7.3	5.1	ft
Maximum Diameter		7.4	7.3	16.8	ft
Total Weight		8,050	6,393	8,300	lb

The NPSS engine model is then used to generate an engine deck, which provides the powerplant's thrust and specific fuel consumption tabulated as a function of aircraft Mach number, altitude, and throttle setting. For a given flight condition, FLOPS interpolates the engine deck to estimate thrust and fuel consumption.

Neither environmental nor cabin noise characteristics are examined in this study, as aircraft acoustic behavior is difficult to capture without high-fidelity geometry and propulsion modeling. Although noise has been a major concern with OR concepts in the past, recent studies suggest modern blade designs can have environmental noise characteristics comparable to those of aircraft in service [15].

B. Engine Placement and Gull Angle

A conventional under-the-wing engine mounting location is chosen to reduce the risk of flutter divergence, minimize interference drag, ensure ease of access for maintenance, and simplify the design of the pylon and airframe [16]. Engine placement beneath the wing is defined by safety and operational considerations.

Unlike turbofans, ORs cannot rely on a nacelle to contain debris in the event of a blade failure. To reduce the risk to passengers and fuselage structural integrity, shielding is installed and the cabin configuration modified. This is discussed in greater detail in Section IV.E. Although the fuselage can be shielded, there is a risk posed by "cross-engine debris" (XED) where a blade fragment from one engine strikes the blades of the opposite engine. The FAA has offered guidance to limit the possibility of cross-engine debris to $1/40^{th}$ of the rotor disk by using the fuselage shielding to block the rest of the path [17]. This constraint is illustrated by the lines labeled "XED" in Fig. 3.

Two ground clearance requirements are imposed to prevent rotor strikes: 5º + 9 in. above the landing gear for crosswind approaches ("X-Wind Approach") and a minimum of one-half engine radius for general ground operations [18]. To minimize flow interactions between the fuselage and rotors, and thus limit acoustic effects and blade fatigue, the distance from the edge of the rotor disk to the fuselage must be a minimum of 70% of the rotor radius ("Fuselage Clearance"). This value is suggested by Vernon et al. [19] for spacing the disk from the wing leading edge (LE) and is applied here to fuselage spacing as well given the inability of lower-order analyses to capture the complexity of these flow interactions.

The engine's forward placement is constrained such that the rotor disk will not strike the ground in the event of a nose gear collapse (NGC). Additionally, the rotor plane of rotation is constrained to be 5º ahead of the root leading edge to prevent blade fragments from impinging on the wing. This is based on the conservative debris spread angle suggested by Raymer [18] and validated by analysis in Ref. [20]. The disk is also required to be a minimum of 70% of the rotor radius ahead of the leading edge at the engine station to reduce blade fatigue caused by the wing's upstream flow effects [19]. These constraints are illustrated in Fig. 3 by the lines labeled "NGC," "Root Clearance," and "Blade Fatigue," respectively.

An engine placement tool was developed using OpenMDAO to reconcile these constraints and place the engine in what is considered the most suitable location. The engine is placed as close to the fuselage as possible to reduce dynamic inertial effects, as well as asymmetrical roll and yaw moments during one engine inoperative (OEI) conditions. To minimize required gull angle, the engine is placed as low to the ground as the constraints will allow. The engine is placed as far aft as possible to minimize its moment on the pylon and impact on center of gravity (CG).

Figure 3 shows the results of the engine placement routine, with active constraints indicated solid lines. The engine's longitudinal location is constrained by the clearance required to reduce blade fatigue. Further aerodynamic analysis may relax this spacing requirement and reduce the engine's forward impact on CG. Interestingly, the dominant constraint on the engine's vertical location, though by a small margin, is cross-engine debris and not ground clearance. Section III.D further examines the structural implications of the XED constraint.

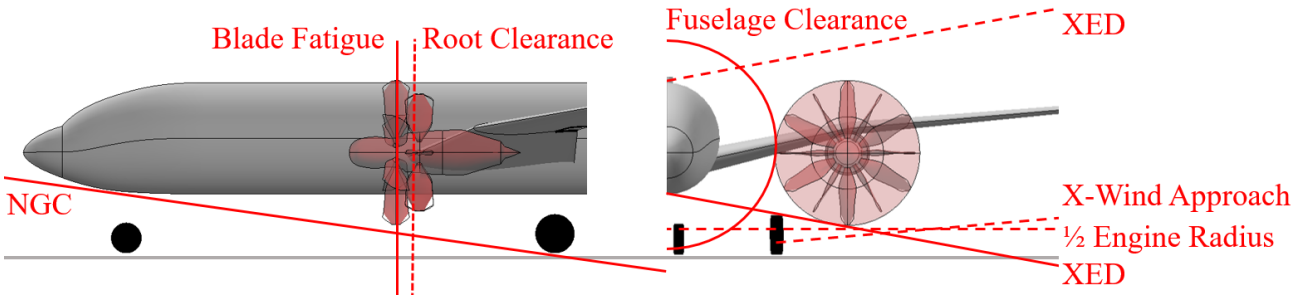

Fig. 3 Diagram of engine placement constraints.

After determining the optimal engine location, Eq. (1) is used to calculate the required inboard dihedral, $\delta_{inboard}$, such that the bottom of the pylon meets the top of the nacelle. Outboard dihedral, $\delta_{outboard}$, is then determined using Eq. (2). This is done to match the roll stability characteristics of the GW154 with those of the baseline and is discussed in greater detail in Section III.F. The parameters in Eqs. (1) and (2) are illustrated in Fig. 4.

$$\delta_{inboard} = \arctan\left(\frac{z_{engine} + r_{nacelle} + dz_{pylon} - z_{wing/root}}{y_{engine} - y_{wing/root}}\right) \tag{1}$$

$$\delta_{outboard} = \frac{\delta_{inboard}(S_{inboard} \cdot y_{MAC/inboard}) + \delta_{avg/Target}(S_{wing} \cdot y_{MAC/wing})}{S_{outboard} \cdot y_{MAC/outboard}} \tag{2}$$

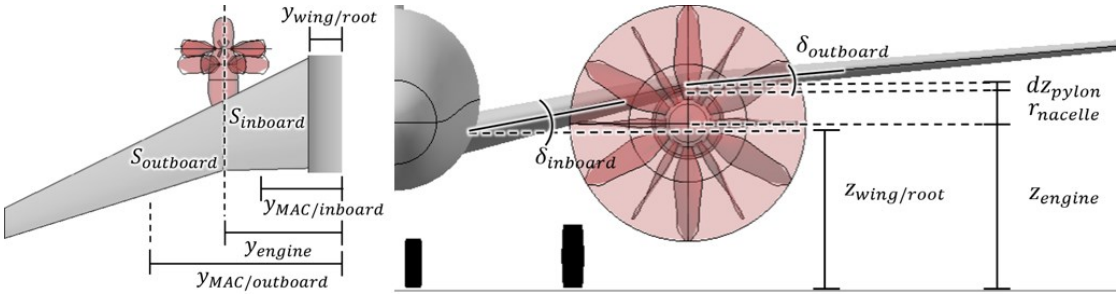

Fig. 4 Parameters relevant to calculating $\delta_{inboard}$ and $\delta_{outboard}$.

For the engine and aircraft geometry used, this placement routine returns a y_{engine} of 20.9 ft, a $\delta_{inboard}$ of 12.4°, and a $\delta_{outboard}$ of 5.5°. It should be noted the wing is considered two discrete sections purely for analysis purposes. Although it may be structurally optimal to join two separate spars rather than manufacture a single curved one, the wing can be lofted to ensure the mold line will curve smoothly and avoid aerodynamic discontinuities.

C. Aerodynamic Modeling

1. Wing Dihedral

The gulled wing's increased inboard dihedral means that for the same airfoil, some additional amount of the lift vector will be lost to the horizontal component. By ignoring finite wing effects and making the simplifying assumption that a wing's vertical lift component, L_z, is directly proportional to its projected area, Eq. (3) can be used to describe the useful lift generated by the wing as a function of its average dihedral δ. The N3CC has a dihedral of 6º. Varying δ from 0º to 18º for the same S_{wing}, there is less than a 5% difference in L_z. Given the low fidelity methods used and the variety of potential solutions (modified airfoil shape, modified planform, increased incidence, or any combination thereof), this difference in vertical lift is considered negligible.

$$L_z \propto S_{wing}\cos(\delta) \tag{3}$$

2. Propulsor-Airframe Interference Effects

To maximize speed for a minimal increase in drag, the wings of cruise-dominated commercial transports are carefully designed for operation close to their Mach drag divergence number, M_{DD}, during cruise [21]. Momentum theory predicts that at cruise thrust and altitude, the rotor will accelerate the flow in its wash to approximately M_{wash}=0.9. As it is impractical to mount a rotor of this size fully beneath a low wing, it is inevitable that some of the

rotor wash will interact with the wing. This interaction results in an altered lift distribution, greater induced drag, and disproportionately increased interference drag in the form of wave drag unless properly accounted for in the wing design.

The greater velocity of the wash relative to the freestream will increase the friction drag acting on the airframe. To quantify the effect of rotor wash on friction drag, friction drag coefficients for power-on and power-off scenarios, $C_{D_{f/power\,on}}$ and $C_{D_{f/power\,off}}$, were determined using Eq. (4), modified from the Empirical Drag Estimation Technique (EDET) employed by FLOPS [22]. Several different approaches exist, but EDET is chosen to ensure a fair comparison against FLOPS-based aircraft models. A summary of the component drag buildup can be found in Table 3, and the relevant parameters are illustrated in Fig. 5. The values for c_{f_c}, FF_c, and k were estimated using tables found in Ref. [22]. These values assume turbulent flow. Aircraft are generally considered to experience fully turbulent flow as historically it has been impossible to predict flow transition points over the course of each mission and the aircraft's lifecycle [22]. Wetted and reference areas were calculated using the OpenVSP geometry. $S_{wet_{wing/wash}}$ and $S_{wet_{wing/clean}}$ were estimated using Eqs. (5) [23] and (6), respectively.

$$C_{D_f} = \sum c_{f_c} \cdot \frac{S_{wet_c}}{S_{ref}} \cdot FF \cdot k \tag{4}$$

$$S_{wet_{wing/wash}} = 2D_{rotor}c_{wash} \tag{5}$$

$$S_{wet_{wing/clean}} = S_{wet_{wing/Total}} - S_{wet_{wing/wash}} \tag{6}$$

Table 3 shows that for the entire aircraft, the net change in friction drag due to rotor wash is thus estimated as $\Delta C_{D_f} = C_{D_{f/power\,on}} - C_{D_{f/power\,off}}$ = + 1 count (one drag count is 1/10,000 of C_D). The N3CC friction drag buildup is also included in the table for comparison. As $C_{D_{f/power\,off}}$ can be internally computed by FLOPS, this small difference is ignored to avoid unnecessary complexity and $C_{D_{f/power\,off}}$ is considered the concept's friction drag coefficient.

Table 3 Comparison of Friction Drag Coefficients, in Drag Counts

Component	$C_{D_{f/N3CC}}$	$C_{D_{f/power\,off}}$	$C_{D_{f/power\,on}}$
Wing	56	71	72
Horizontal Tail	17	16	16
Vertical Tail	11	9	9
Fuselage	66	66	66
Port Nacelle	7	3	3
Starboard Nacelle	7	3	3
Miscellaneous	10	11	11
Total	174	179	180

The N3CC is modeled with a benefit from crossflow-attenuated natural laminar flow (CAT-NLF) over the wing. The GW154 model does not include NLF for several reasons. The crossflow found on highly swept wings has historically limited the application of NLF to transport-category aircraft. The potential benefits of CAT-NLF are difficult to estimate, and an extensive research effort has been undertaken to mature the computational design tools necessary to achieve NLF over the wing [24]. Introducing rotor wash will almost certainly disrupt this flow by adding turbulent air directly to the wing boundary layer. On less swept wings, propeller-induced crossflow velocities have been shown to have a minimal effect on the efficacy of NLF outside of the wash [25]. However, given the natural tendency for outboard sections of swept wings to turn turbulent earlier, the need for detailed computational analysis, and the lack of available test data, it is assumed that the benefits of CAT-NLF cannot be applied to the GW154 and that the gulled wing experiences fully turbulent flow. As seen in Table 3, this constitutes an aerodynamic penalty relative to the N3CC, nominally able to take full advantage of CAT-NLF.

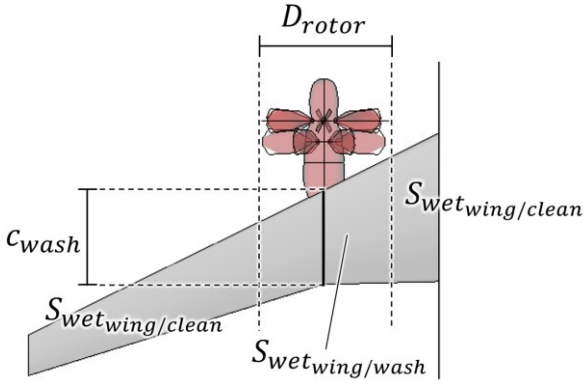

Fig. 5 Parameters relevant to wing friction drag calculations.

The presence of accelerated, helical flow over a transonic wing poses an incredibly complex propulsion integration problem, requiring analysis capabilities well beyond the scope of this paper. Vernon et al. examined how rotor wash affects wing aerodynamics under a similar set of flight conditions [19]. One goal of this research was to determine if the negative flow effects due to rotor wash could be mitigated. The researchers were able to successfully eliminate interference drag and maintain an elliptical lift distribution with negligible loss of lift by modifying the wing planform. A nominal interference drag of $\Delta C_{D_{interference/power\ on}} \approx +10$ counts is assumed for the GW154 to capture the uncertainty surrounding integration effects and the real-world efficacy of wing modifications. This value is the minimum drag reduction presented by the authors for a partially modified wing. For a completely unmodified wing, Vernon et al. provide a useful, though inexact, upper bound of $\Delta C_{D_{interference/power\ on}} \approx +60$ counts.

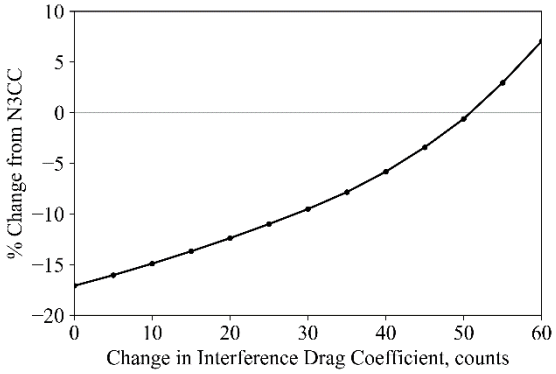

Fig. 6. Sensitivity of GW154 block fuel burn to OR interference drag, as evaluated on a 900 nmi economic mission.

Although the OR-wing aerodynamics are not analyzed in detail in this study, it is useful to understand the GW154 concept's sensitivity to interference drag. This is done by gradually increasing $C_{D_{interference}}$ from zero to 60 in five-count increments and performing mission analysis in FLOPS at each increment. Figure 6 shows that a large amount of interference drag is required to cancel out the VOR's gains from propulsive efficiency. To reduce uncertainty around the integrated effects, there is still a need to improve the understanding of and ability to quantify the aerodynamic interactions between OR engines and airframes.

D. Structural Analysis

Excluding the wing, the weights of all aircraft components were estimated in FLOPS. As with EDET for aerodynamics, these values come from empirical relationships [7]. Though FLOPS gives reasonable weight estimates for conventional wings, the dearth of relevant empirical data and the inability to specify spanwise variations in dihedral within FLOPS's weight equations suggest these estimates may be invalid for a gulled wing.

Lacking any readily available analytical or semi-empirical weight estimation techniques for the specific case of a gulled wing, a mid-fidelity structural analysis and optimization tool known as SUITe of Codes Aeroelastic Sizing using Equivalent plate structural modeling (SUITCASE) is used [26]. SUITCASE is a code developed internally at

NASA's Langley Research Center to predict the structural weight of aircraft concepts from their outer mold line geometry and subsystem weights. Using a 3D model provided by OpenVSP, SUITCASE builds an equivalent plate model of the wing skin and shear web. This plate model is then subjected to a series of load cases in NASTRAN. Aerodynamic forces are determined using an internal vortex-lattice method (VLM) code. The load cases used are specified in Ref. [26]. The results of each analysis iteration are used to minimize the total structural weight, as estimated from total plate volume (the product of plate area and thickness), and material properties.

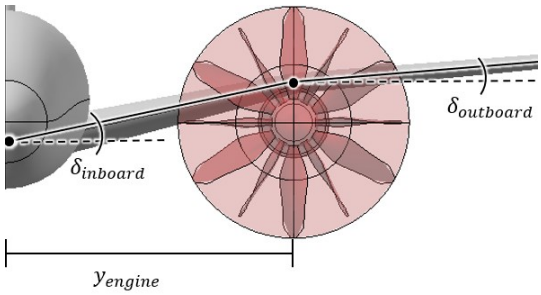

Fig. 7 Diagram of parameters varied in the gull wing structural study.

The N3CC model was first analyzed to provide a baseline weight. The parameters illustrated in Fig. 7, considered the key differentiating factors between gulled and conventional wing weight, were then used to construct a matrix of test points. For consistency of comparison, each wing analyzed had a trapezoidal planform with a projected span of 118.1 ft, a planform area of 1220 ft^2, and LE and trailing edge (TE) sweeps of 26° and 16° respectively. The same aircraft subsystem weights were used for each case to match load factors. The results from these points were compared to the N3CC weight and used to build a surrogate model of wing weight scaling factors relative to the N3CC. For a given wing's dihedrals and engine location, this model interpolates the corresponding scaling factor, which is then passed into FLOPS to adjust its internal estimate. A sample of wing weight sensitivity to the parameters varied can be found in Fig. 8.

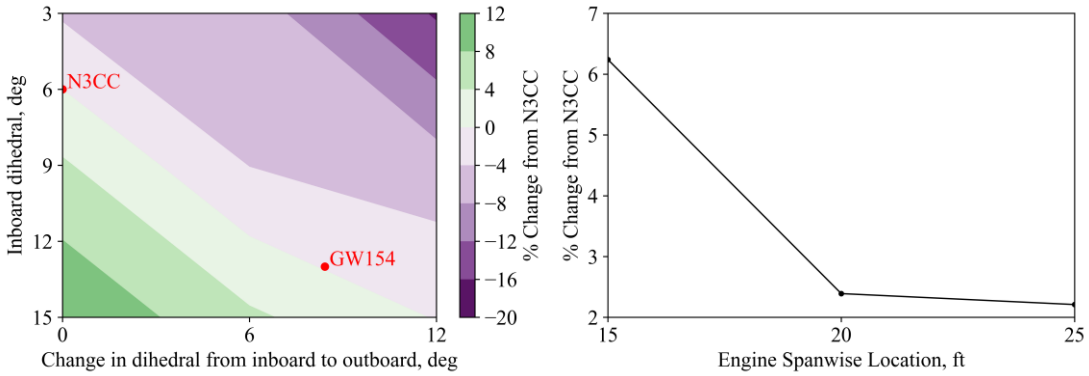

Fig. 8. Sensitivity of gulled wing weight to inboard dihedral and change in section dihedral (left), and spanwise engine location for a constant wing section dihedral of 9° (right).

Interestingly, Fig. 8 shows that SUITCASE estimates wing weight will decrease with greater differences between inboard and outboard dihedral and increase with steeper inboard dihedrals. Upon further investigation there is a stress concentration at the gull joint, exacerbated by the engine mounting. As a result, the SUITCASE optimizer increased plate thicknesses near this point. The subsequent concentration of mass is likely providing static inertial relief, as evidenced by the reduced thicknesses further inboard along the spar carry-through structure. Figure 8 also shows that wing weight trends lower as the engine moves further outboard. This trend is consistent across all dihedrals and changes in dihedral examined. Along with the gull joint mass concentration, increasing engine moment acts to relieve static bending loads in flight. In practice, placing mass further outboard to provide static relief may result in unwanted dynamic effects not captured by the SUITCASE analysis. Given the unintuitive nature of these results, further structural analysis employing higher-fidelity methods is required.

The gull angle had originally been envisioned as a means of integrating large diameter engines without increasing landing gear length. As such, it is useful to understand the tradeoff between achieving distance from the pylon to the

ground, referred to as “pylon height,” with either longer landing gear or a gull angle. Although the gull wing proves convenient for mitigating the risk of cross-engine debris, regulations are subject to change and this constraint may be relaxed in the future. Additionally, future iterations of the GW154 may consider high-diameter turbofans too large to fit below a conventional wing, in which case cross-engine debris would not be a consideration. Figure 9 illustrates the parameters to be varied.

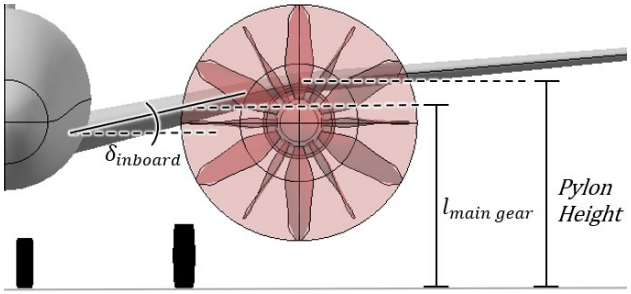

Fig. 9 Diagram of parameters varied in trade between gull angle and landing gear length.

Minimum pylon height is varied from the N3CC value of 9.5 ft to 15.5 ft. For each minimum height constraint, the engine location is determined and the necessary gear length and/or wing dihedrals calculated as a function of aircraft geometry and placement constraints. A positive externality of increased gear length is greater fuselage clearance enabling reduced aft fuselage upsweep. Typically, the rear of the fuselage must be swept upwards to provide sufficient tail clearance on rotation. Viscous flow effects due to this upsweep can account for approximately 15% of total fuselage drag [27]. As landing gear increase in length, greater fuselage clearance allows for reduced aft upsweep and a corresponding reduction in fuselage pressure drag. This aerodynamic benefit is estimated using the methodology outlined in Ref. [28].

Three cases are examined: a conventional case and two gulled wing cases. In the conventional case, referred to as “LG154,” pylon height is achieved solely through extending the landing gear, adjusting its location along the wing as required. In the gulled wing cases, the wing geometry is modified to accommodate clearance requirements and the landing gear is altered to match this new wing geometry. This modified wing geometry corresponds to a change in weight, estimated using the surrogate model discussed above. The two gulled-wing cases are run with and without the XED constraint active to better understand the aircraft-level impact of this constraint.

The calculated landing gear lengths, wing weight factors, and modified fuselage drags are used to override FLOPS internal estimates. Figure 10 presents a side-by-side comparison of the GW154 with the XED constraint active and the LG154 at the design point. The results of this study are presented in Fig. 11. A gulled wing achieves the same distance from pylon to ground with a shorter and lighter landing gear. The increase in main gear lengths for both gulled wing cases is delayed due to other constraints defining a wing geometry that already satisfies the minimum pylon ground clearance. Additionally, gulled wing gear length increases at a slower rate as pylon height is achieved by modifying wing geometry. This increase in length is due to the steeper dihedrals moving the wing further from the ground. Removing the XED constraint allows for even shorter landing gear but has a negligible impact on overall performance.

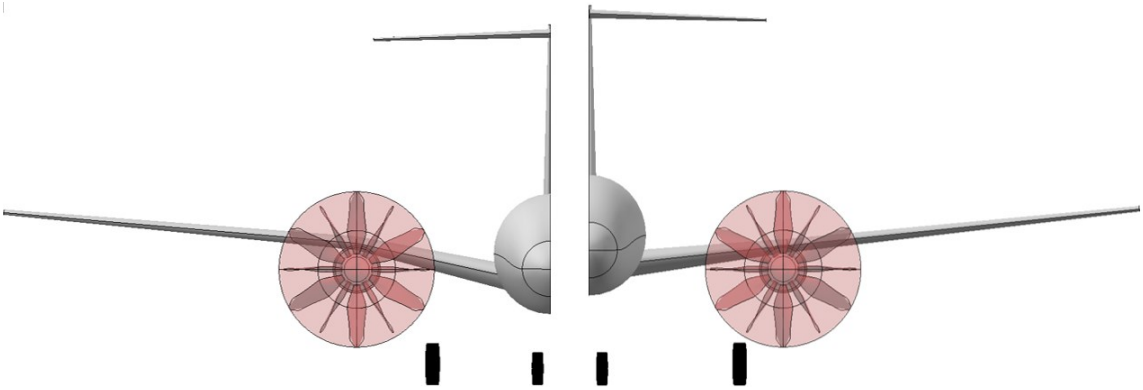

Fig. 10 Front view comparison of the GW154 (XED constraint active) and LG154 at the design point.

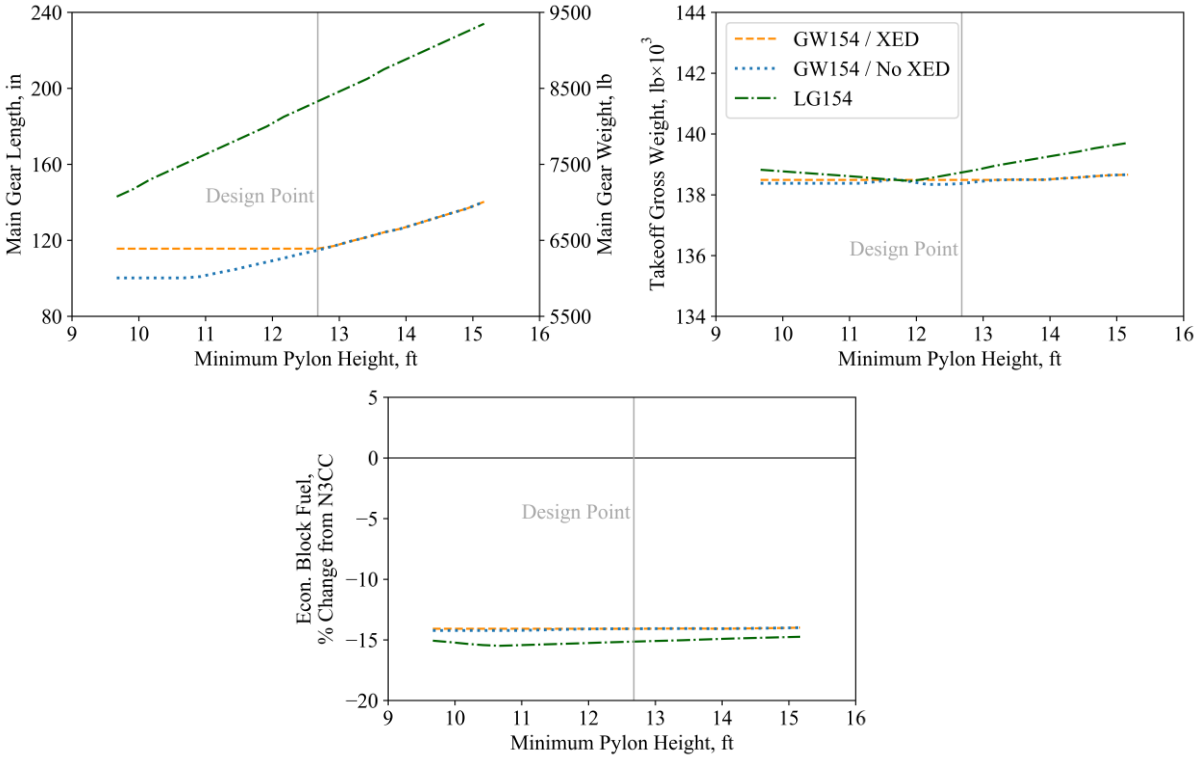

Fig. 11 Results of landing gear length study, as evaluated with the VOR.

There is an inflection in the slope of the TOGW curve from negative to positive slope for the LG154. This occurs at a pylon height of approximately 12 ft and is due to the fuselage upsweep, and thus its drag contribution, being entirely removed. With no further drag benefit to be claimed, the LG154 slope becomes steep compared to the gulled wing concepts. This increased slope indicates that as engines increase in diameter, landing gear concepts trend heavier than their gulled wing counterparts.

Only the LG154 shows a response in TOGW to pylon height. The gulled wing results in reduced TOGW, though only by a small margin. None of the concepts' economic block fuel burns exhibit a pronounced sensitivity to pylon height. Due to its reduced fuselage drag, the LG154 burns less fuel than the GW154 concepts on the economic mission. This benefit is on the order of 1%.

An additional consideration is that longer landing gear can pose significant configurational and operational penalties not captured in this analysis. They require a greater proportion of internal volume and must be placed further outboard. This reduces available space for cargo and fuel, increases turning radius during taxi, and can require engines to be placed further outboard at the expense of a greater OEI moment. Drastically increasing their size and weight will complicate maintenance of both the gear itself and the aircraft, as the fuselage will be further off the ground. Landing gear also contribute a large proportion of airframe noise. In an OR configuration, noise must be carefully considered, and increased gear size will only further exacerbate this concern.

E. Fuselage Shielding

The high rotational energy contained in open rotor blades and their unproven safety record necessitate the use of fuselage shielding. A set of studies summarized by Ref. [17] developed a methodology to estimate minimum shielding thickness as a function of blade energy, impact angle, and shielding material properties. These estimates were experimentally validated on a triaxially-braided composite shield using FAA-provided blade geometry and flight conditions representative of those anticipated for this concept. The relevant composite material properties and testing conditions used can be found in Ref. [29]. The minimum amount of energy that the shield must absorb, E_A, is set equal to blade kinetic energy. Without detailed propulsion data, blade kinetic energy is taken directly from Ref. [20]. Applying a factor of safety (FS) of 1.25 on the load applied to the shielding, Eq. (7), taken from Ref. [29], results in an estimated minimum shielding thickness of 0.66 in. This FS is based on the FAA guidance for "major engine structural failure events," found in Ref. [30].

$$t_{shielding} = \sqrt{\frac{12E_A \cos^2\theta_{impact}}{LT}} \tag{7}$$

Table 4 Values for Shielding Weight Estimate [20]

Parameter	Symbol	Value	Units
Shielding Density	$\rho_{shielding}$	0.0645	lb/in^3
Fuselage Circumference	$C_{fuselage}$	40.8	ft
Debris Radius	r_{debris}	14.9	ft
Debris Spread Angle	θ_{debris}	5	degrees
Shielding Thickness	$t_{shielding}$	0.66	in

Although it may be possible to vary the shielding thickness around the fuselage circumference depending on expected impact angle to minimize weight, the multitude of unknowns during an actual flight mean this may not be a valid assumption [20,31]. Thus, the entire fuselage circumference in the debris path is considered to have full-thickness shielding. For the purposes of this analysis, the fuselage is assumed to be a circle of diameter $D_{fuselage}$= 13 ft. Using the engine placement results and the values found in Table 4, Eq. (8) is then applied to calculate a total shielding weight of 652 lb. Figure 12 illustrates a diagram of these parameters.

$$w_{shielding} = \rho_{shielding} \cdot \left(2r_{debris} \tan\theta_{debris} \cdot C_{fuselage} \cdot t_{shielding}\right) \tag{8}$$

The shielding is conformally integrated into the fuselage to avoid aerodynamic penalties. No details on mounting structure requirements were available; however, because of the conservative approach taken to estimate shielding weight, the mounting weight is assumed to be negligible.

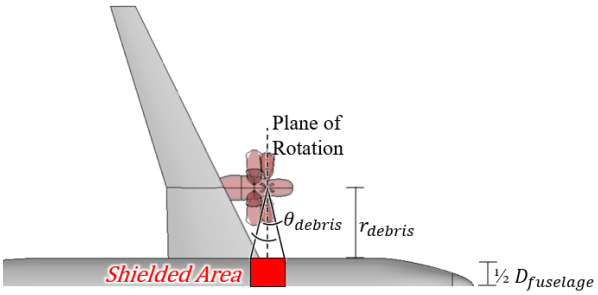

Fig. 12 Diagram of approach to shielding weight estimate. (Not to Scale)

F. Stability and Control

A T-tail empennage is required to keep critical control surfaces out of the rotor wash. Tail sizing is driven by empirically derived volume coefficients, which can be found in Ref. [32]. The control surface analysis methodology outlined in Ref. [33] is implemented to ensure the vertical tail is sufficiently large to satisfy OEI conditions, approximated by the moment of one engine at maximum takeoff thrust.

Roll stability provided by dihedral is primarily dependent upon two factors: the lift produced by the wing and the moment arm at which it acts. The lift of each section is considered proportional to its area and is assumed to act at the spanwise station of the section mean aerodynamic chord (MAC). Equation (2) is developed from these assumptions to determine the outboard dihedral required such that the average total moment resulting from each section's dihedral equals that of the baseline.

V. Sizing and Mission Analysis Methodology

The analysis framework for this concept is shown in Fig. 13. It is assumed that the GW154's wing, as with most transports of this category, is sized by takeoff and climb constraints. To achieve takeoff and climb performance similar to the N3CC, the wing loading of the GW154 is matched to the baseline. Concept wingspan is limited to a maximum of 118.1 ft due to airport gate constraints; therefore, span is held constant and the wing area is modified exclusively through chord. The wing area and aircraft weights will change, and thus CG location will change as the aircraft is

iterated upon. To account for the impact of this shift on stability, the empennage is sized using the approach described in Section III.F.

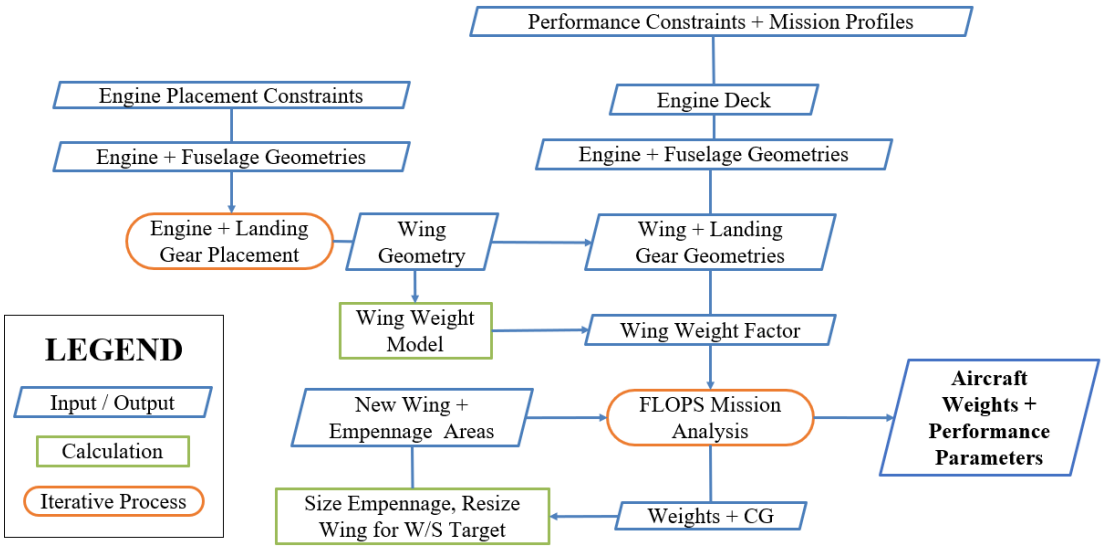

Fig. 13 Flowchart of aircraft analysis methodology

Thrust-to-weight ratio (TWR) is not matched between concepts as part of this sizing routine. Although FLOPS can scale an engine to the dimensions, weights, and fuel flows that would be required to meet a specified thrust target, these scaling relationships were developed for turbofan engines and their validity for ORs has not been investigated [7]. Powered by an oversized VOR, the GW154 has a TWR approximately 20% greater than that of the N3CC. The ability to scale OR powerplants would likely result in a slightly smaller and lighter VOR.

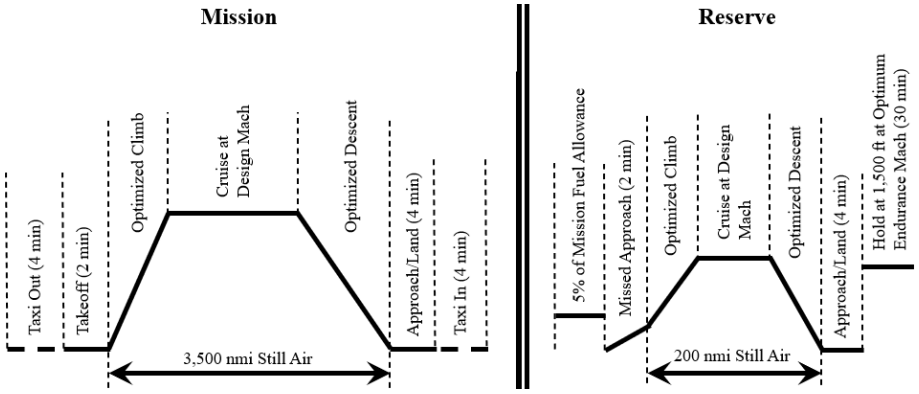

Fig. 14 Example of mission profile with which the GW154 is evaluated.

FLOPS is used to estimate overall aircraft weight and perform mission analysis. The aircraft model is sized based on a 3,500 nmi design mission and is subsequently evaluated at several ranges below this maximum to contextualize performance across the breadth of expected missions. Particular focus is given to the nominally 900 nmi "economic mission" representative of the routes narrowbodies typically fly. Figure 14 shows the design mission profile defined for FLOPS analysis. All missions run by FLOPS follow this form.

VI. Results

Three concept variants are examined, and their performance is compared to that of the N3CC. The GW154, as the focus of this study, is evaluated with both the AT and VOR engines. The AT variant, GW154-AT, employs the gulled wing required by the VOR to isolate the effects of the configuration itself. The LG154 is also included to better understand the potential of an OR concept integrated onto a more conventional configuration. These concepts are modeled in FLOPS and compared in two separate cases: one with nominal assumptions (NLF on the N3CC and GW154-AT, but not OR concepts) and one with no NLF effects present on any aircraft.

As seen in Fig. 15, the gulled wing itself has a minor positive impact on fuel burn due to reduced wing and landing gear weights. Thus, a large portion of the differences in performance between the OR and advanced turbofan concepts can be attributed to the integrated effects of the VOR. However, the wing structural weight benefit requires validation.

Both VOR concepts exhibit a clear advantage across the board relative to the AT. Given nominal assumptions, the benefits of an OR are most apparent on shorter missions. This is because these engines perform better than their turbofan counterparts at lower altitudes and speeds. As discussed in Section III.D, the LG154 achieves slightly lower block fuel burn than the GW154 due the aerodynamic benefit of reduced upsweep. This relative advantage is narrow in large part due to the LG154's increased landing gear weight.

If the N3CC is unable to take full advantage of CAT-NLF, the relative fuel burn advantage of the OR concepts increases with range. Should CAT-NLF benefits not be fully realized or should an OR concept be able to take advantage of some level of NLF over the wing, ORs will certainly gain an increased competitive edge.

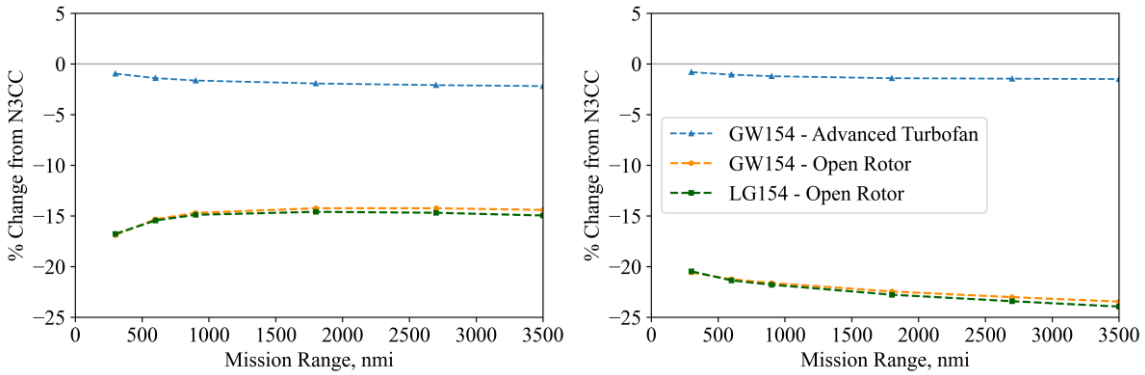

Fig. 15 Comparison of concept fuel burn estimates with nominal NLF assumptions (left) and with no NLF applied to any concepts (right).

Table 5 Concept Performance Parameters

Parameter	N3CC	GW154-AT	GW154	LG154	Units
Wing Area	1220	1199	1211	1238	ft^2
Landing Gear Length	108	90	116	193	in
Landing Gear Weight	5703	5244	5828	7690	lb
Shielding Weight	0	0	652	652	lb
EW	68,405	66,904 (-2%)	71,544 (+5%)	74,833 (+10%)	lb
TOGW	138,292	136,147 (-2%)	137,238 (-1%)	140,350 (+1%)	lb
Design Mission Fuel	30,366	29,708 (-2%)	25,922 (-15%)	25,826 (-15%)	lb
Econ Mission Fuel	8,090	7,958 (-2%)	6,902 (-15%)	6,886 (-15%)	lb

Parameters of interest for the concepts evaluated can be found in Table 5. For a small increase in landing gear length, the GW154 effectively integrates the VOR, reducing both aircraft fuel burn and weight relative to the N3CC. The increases in EW and TOGW for the LG154 can be largely attributed to the longer landing gear.

It is important to note that these results are dependent on the assumptions made to arrive at them. More research on both the enabling technologies and the integrated effects of ORs is required to fully understand their aircraft-level impacts. As the body of knowledge surrounding this promising technology grows, so too will our confidence in the true nature of its relative benefits.

VII. Concluding Remarks

Using low- and mid-fidelity analyses, two aircraft configurations integrating an open rotor engine were modeled. The weights and mission block fuel burns of these models were calculated and then compared to a conventional configuration baseline to understand the aircraft-level impacts of open rotor powerplants.

This work highlights the potential of OR engines to reduce aviation emissions. Gulled wing configurations appear to remain competitive against more conventional peers as a means of effectively integrating large diameter

powerplants. The unintuitive reduction in wing weight following the addition of a gull angle merits further investigation. Even with a greater TOGW than the GW154, the LG154 concept demonstrated a small fuel burn advantage due to a reduction in fuselage drag. However, there are operational and configurational penalties associated with the required increase in landing gear length. On the other hand, a gulled wing will likely pose manufacturing challenges not addressed in this study. Given the marginal difference in performance, the choice between long landing gear and a gulled wing may come down to manufacturer and operator preferences.

Conservative assumptions were made affecting nearly every aspect of this analysis due to the low fidelity tools and methods available for the preliminary design of OR-driven concepts. The negative factors affecting fuel burn were the lack of laminar flow over the wing, increased engine weight, shielding weight, and rotor-airframe interference drag. Despite a conservative approach, ORs still appear to have an appreciable reduction in fuel burn. Differences between the assumptions made to develop the AT and VOR models accounts for some uncertainty in the fidelity of these results.

Alternate configurations may better capitalize on OR technology. In addition to investigating these concepts, the author envisions three primary areas of focus for future work: incorporating low-speed performance modeling, higher-fidelity structural analysis, and improved propulsion modeling. These will enable a higher level of certainty in the results and a greater understanding of the integrated potential of open rotor engines.

Acknowledgments

The author thanks the Advanced Air Transport Technologies (AATT) and Hybrid Thermally Efficient Core (HyTEC) projects for funding this effort. The author also thanks Jeffryes Chapman and Michael Bennett for providing a propulsion model, and Ty Marien for his guidance through this work.

References

[1] Klöwer, M., Allen, M. R., Lee, D. S., Proud, S. R., Gallagher, L., and Skowron, A., "Quantifying aviation's contribution to global warming," *Environmental Research Letters* [online journal], Vol. 16, No. 10. DOI: 10.1088/1748-9326/ac286e [retrieved 19 April 2024].

[2] Graver, B., Rutherford, D., and Zheng, S., "CO2 Emissions from Commercial Aviation, 2013, 2018, and 2019," International Council on Clean Transportation, Washington, DC, Oct. 2020.

[3] Guynn, M. D., Berton, J. J, Tong, M. T., and Haller, W. J., "Advanced Single-Aisle Transport Propulsion Design Options Revisited," AIAA Paper 2013-4330, August 2013. DOI: 10.2514/6.2013-4330

[4] Hardiman, J., "How do the Boeing 737 MAX 10's Extended Wheels Work?," *Simple Flying* [online article], Sep. 2021. URL: https://simpleflying.com/boeing-737-max-10-extending-landing-gear/ [retrieved 16 April 2024]

[5] Welstead, J., and Felder, J. L., "Conceptual Design of a Single-Aisle Turboelectric Commercial Transport with Fuselage Boundary Layer Ingestion," AIAA 2016-1027, 2016. DOI: 10.2514/6.2016-1027

[6] McDonald, R. A., and Gloudemans, J. R., "Open Vehicle Sketch Pad: An Open Source Parametric Geometry and Analysis Tool for Conceptual Aircraft Design," AIAA Paper 2022-0004, Jan. 2022. DOI:10.2514/6.2022-0004

[7] Wells, D. P., Horvath, B. L., and McCullers, L. A., "The Flight Optimization System Weights Estimation Method," NASA TM-2017-219627, 2017.

[8] Gray, J. S., Hwang, J. T., Martins, J. R. R. A., Moore, K. T., and Naylor, B. A., "OpenMDAO: An Open-Source Framework for Multidisciplinary Design, Analysis, and Optimization," *Structural and Multidisciplinary Optimization*, Vol. 59, 2019, pp. 1075-1104. DOI: 10.1007/s00158-019-02211-z

[9] Chapman, W.C., Bennet, M., and Tong, M., "Performance and Weight Estimates of an Open Rotor Propulsion System Concept for Next Generation Aircraft," AIAA SciTech 2025 (submitted for publication)

[10] "CFM RISE Program White Paper," CFM International, July 2021. URL: https://www.cfmaeroengines.com/wp-content/uploads/2021/07/CFM_RISE_Whitepaper_Media.pdf [retrieved 15 April 2024]

[11] Kroo, I. "Propeller-Wing Integration for Minimum Induced Loss," *Journal of Aircraft*, Vol. 23, No. 7, 1986, pp. 561-565. DOI: 10.2514/3.45344

[12] Veldhuis, L. L. M., "Review of Propeller-Wing Aerodynamic Interference," *24th International Congress of the Aeronautical Sciences, Yokohama, Japan,* ICAS 2004-6.3.1, 2004.

[13] Lytle, J. K., "The Numerical Propulsion System Simulation: An Overview," NASA TM 2000-209915, 2000.

[14] Tong, M. T., and Naylor, B. A., "An Object-Oriented Computer Code for Aircraft Engine Weight Estimation," NASA TM 2009-215656, 2009.

[15] Hendricks, E. S., Berton, J. J., Haller, W. J., Tong, M. T., and Guynn, M. D., "Updated Assessment of an Open Rotor Airplane Using an Advanced Blade Design," NASA TM-2013-218074, 2013.

[16] Blaesser, N. J., "Interference Drag Due to Engine Nacelle Location for a Single-Aisle, Transonic Aircraft," Ph.D. Dissertation, Aerospace and Ocean Engineering Dept., Virginia Polytechnic Institute, Blacksburg, VA, 2019.

[17] Seng, S., Frankenberger, C., Ruggeri, C. R., Revilock, D. M., Pereira, J. M., Carney, K. S., and Emmerling, W. C., "Dynamic Open-Rotor Shield Impact Test Report," NASA TM-2015-218811, 2015.

[18] Raymer, D. P., *Aircraft Design: A Conceptual Approach*, 5th ed., AIAA Education Series, AIAA, Reston, VA, 2012. Chap. 10.

[19] Vernon, D. F., Page, G. S., Welge, H. R.., "Propfan Experimental Data Analysis," NASA CR-166582, 1984.

[20] Carney, K., Pereira, J. M., Kohlman, L., Goldberg, R., Envia, E., Lawrence, C., Roberts, G., and Emmerling, W., "Weight Assessment for Fuselage Shielding on Aircraft with Open-Rotor Engines and Composite Blade Loss," NASA TM-2013-216582, 2013.

[21] Harris, C. D., "NASA Supercritical Airfoils: A Matrix of Family-Related Airfoils," NASA TP-2969, 1990.

[22] Feagin, R. C., and Morrison, W. D., "Delta Method, an Empirical Drag Buildup Technique," NASA CR-151971, 1978.

[23] Dorsey, A., and Uranga, A., "Design Space Exploration of Future Open Rotor Configurations," AIAA Paper 2020-3680, August 2020. DOI: 10.2514/6.2020-3680

[24] Lynde, M. N., Campbell, R. L., Hiller, B. R., Owens, L. R., "Design of a Crossflow Attenuated Natural Laminar Flow Flight Test Article," AIAA Paper 2021-0173, January 2021. DOI: 10.2514/6.2021-0173

[25] Howard, R. M., Miley, S. J., Holmes, B. J., "An Investigation of the Effects of the Propeller Slipstream on a Laminar Wing Boundary Layer," SAE Paper 850859, January 1985. DOI: 10.4271/850859

[26] Horvath, B. L., and Wrenn, G. A., "Development of an Inertia Relief Method for Aircraft with Dissimilar Engines in LEAPS," AIAA Paper 2021-2434, July 2021. DOI: 10.2514/6.2021-2434

[27] Ouyang, S., Liu, Y., Zhaeo, X, Zhang, X., "The Research on the Drag Reduction of Transport Aircraft Using Ventral Fins," *The Proceedings of the 2018 Asia-Pacific International Symposium on Aerospace Technology*, APISAT, Chengdu, China, 2018, pp. 1515-1525. DOI: 10.1007/978-981-13-3305-7_121

[28] Shevell, R., Notes on Drag Analysis, Stanford University, 1974.

[29] Lundin, S. J., and Mueller, R. B., "Advanced Aircraft Materials, Engine Debris Penetration Testing," DOT/FAA/AR-03/37, Dec. 2005.

[30] Federal Aviation Administration, "Engine Failure Loads," FAA AC No. 25.362-1, Dec. 2014/

[31] Federal Aviation Administration, "Minimizing the Hazards from Propeller Blade and Hub Failures," FAA AC No. 25.905-1, Sep. 2000.

[32] Morris, J., Ashford, D.M., "Fuselage Configuration Studies," SAE Technical Paper 670370, 1967. DOI: 10.4271/670370

[33] Nicolosi, F., Ciliberti, D., Vecchia, P.D., Corcione, S., and Cusati, V., "A Comprehensive Review of Vertical Tail Design," Department of Industrial Engineering, University of Naples, Naples, Italy, September 2016. DOI:10.13140/RG.2.2.12606.69448